

RESEARCH ARTICLE



ISSN: 2321-7758

STRUCTURAL AND MAGNETIC PROPERTIES OF Mn-Ni-Zn NANOFERRITES DOPED WITH Ce³⁺ SYNTHESIZED BY SOL-GEL METHOD

THUMMAPUDI NIRANJAN KUMAR¹, CH. VIJAY ANIL DAI² K.SURESH³

¹Lecture in physics, AMAL College Anapalli, Visakhapatnam, Andhra Pradesh

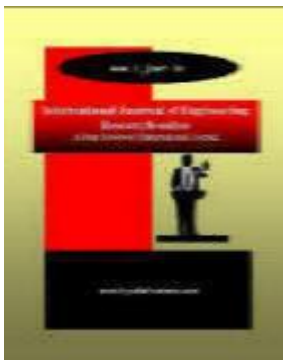
²Lecture in physics, A.G & S.G Siddhartha College of Arts and Science, Vuyyuru, Krishna, A.P

³Lecture in Physics, VSR & NVR Degree College, Tenali, Guntur Dist., A.P., India

Article Received: 17/06/2013

Article Revised: 20/8/2013

Article Accepted: 31/08/2013



ABSTRACT

Nanostructured Mn–Ni–Zn ferrites with composition Mn_{0.2} Ni_{0.6} Zn_{0.5} Ce_x Fe_(2-x) O₄ (where x = 0.02, 0.04, 0.06, 0.08) have been prepared by sol–gel method. The structural data obtained by X-ray diffraction (XRD) of all Mn–Ni–Zn nanoferrites confirmed the spinel structure. Single phase spinel ferrite of Mn nanoferrites were examined using X-ray diffraction (XRD) analysis whereas the multiphase structure was observed as Ce³⁺ contents increased from x = 0.04. Scanning electron microscopy (SEM), and Fourier transform infrared spectroscopy (FTIR) were used to find out the morphology phase and metal stretching vibrations of Ce³⁺ substituted nanocrystalline ferrites. The crystallite size was increased and found in the range of 32-40 nm. The agglomerations in Mn ferrite samples decrease as the Ce³⁺ concentration increases. The magnetic properties such as remanence, saturation magnetization, coercivity, Bohr magneton and magnetocrystalline anisotropy constant (K) were determined using M–H loops recorded from a vibrating sample magnetometer (VSM). Saturation magnetization, remanence and coercivity are decreased as the Ce³⁺ contents increase in Mn nanocrystalline samples. Cerium doped Manganese nanocrystalline ferrites with excellent properties may be suitable for potential applications in sensing, security, switching, core, multilayer chip inductor, biomedical and microwave absorption applications.

©KY PUBLICATIONS

INTRODUCTION

Mixed manganese/Cerium ferrites having high Curie temperatures and magnetization depending on the composition form an important class of magnetic materials used in many technological application¹. The magnetic particles with smaller size become single domain in contrast with the usual multi domain structure for bulk magnetic material exhibiting superparamagnetization. Magnetic particles exhibiting superparamagnetic behavior display higher saturation magnetization and low coercivity having potential applications e.g., as magnetic resonance imaging contrast agents, in ferrofluids based technology, information storage device, gas sensors. Magnetic particles with sizes in the nanometer scale are now of interest because of their many technological applications and unique magnetic properties which differ considerably from those

of bulk materials. Below a critical size, magnetic particles become single domain in contrast with the usual multi domain structure of the bulk magnetic materials, thus exhibiting unique phenomena such as super paramagnetic and quantum tunneling of the magnetization. Magnetic nano particle systems exhibiting super paramagnetic behavior, display little or no remanence and coercivity while keeping a very high saturation magnetization².

Both Mn–Zn and Ni–Zn ferrites have a great importance from the application point of view, where they are used in many ferrite devices such as inductor cores, converters, magnetic heads, and electromagnetic wave absorbers. Although Mn–Zn ferrites have distinctive magnetic properties as high initial permeability and magnetization, they have low electrical resistivity and high power losses. So, they are not suitable for magnetic applications especially at high frequencies. On the other hand, Ni–

Zn ferrites are characterized by their high resistivity, low dielectric loss and high Curie temperature, but they have relatively low initial permeability at high frequencies. Combinations between these two ferrites were carried out by many studies trying to obtain favorable magnetic properties with low losses especially at high frequencies in bulk and powder forms³. In a previous work, the magnetic and electrical properties of such a combination were investigated⁴. The sample with the chemical formula $Mn_{0.5}Ni_{0.1}Zn_{0.4}Fe_2O_4$ was found to possess the optimum properties for promising applications. Moreover, it was noticed clearly that the properties of Mn–Ni–Zn ferrites are predominantly governed by the type of substituted ions⁵. Accordingly, this work deals with the improvement of the magnetic properties of this last optimum sample when Ce^{3+} ions substitute only Fe^{3+} ions. This may present a candidate for magnetic applications in high frequency field.

Materials and Method

Nanoferrites synthesis: $Mn_{0.2} Ni_{0.6} Zn_{0.5} Ce_x Fe_{(2-x)} O_4$ (where $x = 0.02, 0.04, 0.06, 0.08$) nano ferrites were synthesized by sol–gel auto-combustion technique⁶ by varying the Ce^{3+} ion concentration using AR grade (99% pure) purchased from SD fine chemicals, India. To obtain homogenous and transparent solution, citric acid was used as a chelating agent. Dissolved solution was mixed homogeneously by placing it on magnetic stirrer at the temperature of 90°C. pH value was maintained at 7.5–8.5 by adding ammonia solution continuously followed by stirring for 5–6 hours. The solution transformed into viscous gel first and then a self combustion phenomenon occurred at temperature 400°C. Dry gel converted into fluffy powder called “Preliminary powder” after its complete burning. The powder, after complete grinding, was then pre-sintered at 750 °C in a furnace for 4 hours, followed by furnace cooling. These sintered powders were then pressed into pellets under the load of (~30 KN) by using Paul–Otto Weber Hydraulic Press. The pellets were formed using (3–5 wt %) polyvinyl alcohol as a binder. The binder was evaporated at 250°C for 2 hour and finally samples were sintered again at 1000°C for 5 hours.

Structural characterization

X-Ray Diffraction (XRD): X-ray diffraction is now a common technique for the study of crystal structures and atomic spacing. The patterns for the MnO nanoparticles were recorded using an X-ray diffractometer (PANLYTICAL) using secondary monochromatic Cu $K\alpha$ radiation of wavelength $\lambda = 0.1541$ nm at 40 Kv/50 mA in the scan range $2\theta = 20^\circ$ to 90° . Samples were supported on a glass slide.

Scanning Electron Microscopy (SEM): Morphology of the samples was investigated using scanning electron microscope (model JSM-7000F) which also has been used for compositional analysis of the prepared MnO nanoparticles. A drop of nanoparticles dissolved in methanol was placed on a copper grid.

Fourier Transform Infrared Spectroscopy (FTIR): The fourier transform infrared (FTIR) absorption spectra of the samples were recorded using FTIR spectrometer (Thermo Nicolet, Avatar 370) in the wave number range $4000\text{--}400\text{ cm}^{-1}$ with Potassium bromide (KBr) as binder.

The magnetic characterization was carried out using a Vibrating Sample Magnetometer (VSM; Lakeshore 7410) at room temperature up to a maximum field of 20 kOe.

RESULTS AND DISCUSSION

X-ray diffraction patterns, (Figure 1), showed that all the investigated samples have single cubic spinel phase. The all measured XRD peaks match well with the standard patterns (JCPDS) of cubic spinel ferrite. Interplane distance and planes are calculated by Bragg's diffraction law and index method using equation 1 & 2. The Ce³⁺ doped Mn-Ni-Zn nanoparticles exhibit several diffraction peaks which can be indexed as cubic structure. The average crystalline size of the prepared Mn-Ni-Ce-Zn nanoferrite particles was found in the range of 32-40 nm for 750° c for the composition of (where x= 0.0, 0.02,0.04, 0.06 & 0.08) , by using Sherrer's formula. The intensity & width of the Bragg's peak Conforming good crystallinity & nano particle size it is also good agreement with research article.

The interplane distance were calculated by using bragg's equation from the relation

$$n\lambda = 2d \sin \theta \dots (\text{Eqn...1})$$

The lattice parameter "a" was calculated using following relation

$$a = d\sqrt{h^2 + k^2 + l^2}$$

Where (hkl) is the miller indices, λ is the wavelength of X-ray radiation and θ is the Bragg angle. The results of interplane distance and lattice parameter are shown in table 1. The particle size were calculated using Scherrer's formula

$$t = \frac{0.9\lambda}{\beta \cos \theta}$$

here, "t" is the particle size, and β is the FWHM (full width half maxima) of the peak θ Value of lattice constant for x=0.0 comes out to be 8.235Å, well in agreement with reported value. The decrease in value of the lattice parameter with doping suggests that there is shrinkage in unit cell. The single phase cubic spinel structure was clearly indicated by the XRD patterns of pure Mn-Ni-Zn-Ce nanoferrites. The XRD pattern also shows that all the samples had formed the cubic single phase spinel structure.

Table 1: Effect of Ce³⁺ substitution on the lattice parameter, crystallite size, X-ray density, and lattice strain of Mn_{0.2}Ni_{0.6}Zn_{0.5}Ce_xFe_(2-x)O₄

Ce ³⁺ substituted Nanoferrites (x)	Lattice parameter (Å)	Crystallite size (nm)	X-ray density (g cm ⁻³)	Lattice strain %
Mn _{0.2} Ni _{0.6} Zn _{0.5} Fe ₂ O ₄	8.235	32.1 ±1.2	5.106	-0.197
Mn _{0.2} Ni _{0.6} Zn _{0.5} Ce _{0.02} Fe _(2-0.02) O ₄	8.203	38.4 ±1.6	5.357	0.194
Mn _{0.2} Ni _{0.6} Zn _{0.5} Ce _{0.04} Fe _(2-0.04) O ₄	8.164	40.1 ±1.1	5.449	0.066
Mn _{0.2} Ni _{0.6} Zn _{0.5} Ce _{0.06} Fe _(2-0.06) O ₄	8.184	41.2 ±1.3	5.541	-0.035
Mn _{0.2} Ni _{0.6} Zn _{0.5} Ce _{0.08} Fe _(2-0.08) O ₄	8.192	45.5 ±1.0	5.642	0.104

Values of the lattice parameter (a) were calculated according to the procedure mentioned before⁷. Figure 2 shows the variation of the lattice parameter as a function of Ce-concentration (x). It can be seen that the lattice parameter decreases dramatically with the Ce-concentration up to x= 0.04 then it becomes nearly constant for 0.02 < x ≤ 0.08. For x ≤ 0.04, the decrease in the lattice parameter could be attributed to that some rare earth ions reside at the grain boundaries⁸. Hence, they hinder the grain growth and may exert a pressure on the grains and lead the lattice parameter to decrease.

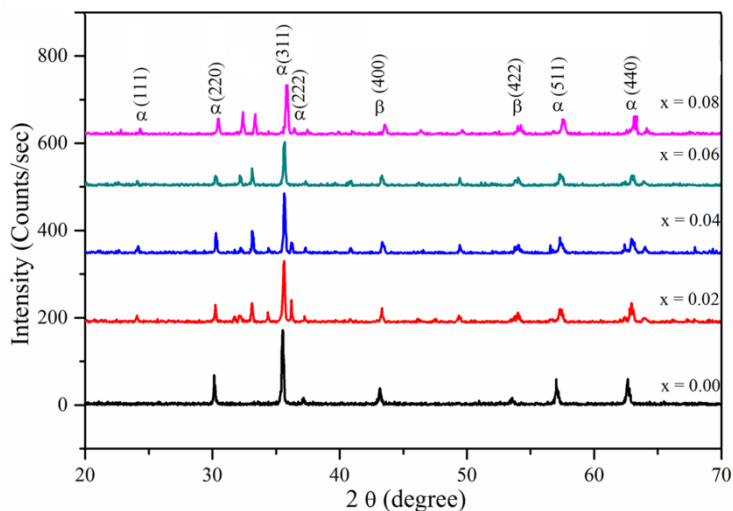


Figure 1: X-ray diffraction patterns for $\text{Mn}_{0.2}\text{Ni}_{0.6}\text{Zn}_{0.5}\text{Ce}_x\text{Fe}_{(2-x)}\text{O}_4$ (where $x = 0.00, 0.02, 0.04, 0.06, 0.08$)

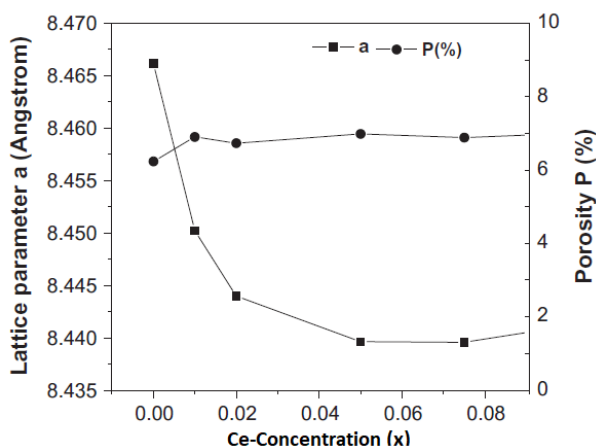


Figure 2: Variation of the lattice parameter a (\AA) and Porosity P (%) with Ce^{3+} concentration (x).

FT IR spectral studies

Figure 3 shows the room temperature IR spectrum of the above mentioned samples. The spectra are recorded in the range 400 to 4000 cm^{-1} . The spectra show two main absorption bands below 1000 cm^{-1} which is a common feature of ferrites. The high frequency band lies in the range 560 – 600 cm^{-1} while the low frequency band ν_1 lies in the range 474 – 436 cm^{-1} . These bands are assigned to the vibrations of the metal ion-oxygen complexes in tetrahedral and octahedral sites, respectively⁹. It is observed that the high frequency band ν_1 increases with increase in Ce^{3+} substitution, whereas the low frequency band ν_2 is found to decrease. Waldron¹⁰ attributed the high frequency band to the intrinsic vibrations of the tetrahedral groups and the low frequency band to the octahedral groups. Puri and Varshney¹¹ have reported that Zn^{2+} showed a strong preference for tetrahedral A site and Ni^{2+} ion showed preference for B site, while Mn^{2+} ions showed preference for A site and B site. We have also observed from our earlier studies¹² that Ni^{2+} ions occupy the B site and force some of the Fe^{3+} ions from B site to A site. Ni^{2+} ions in the octahedral site have larger ionic radius and higher atomic weight than Fe^{3+} ions. This affects the Fe^{3+} -O⁻ stretching vibration resulting in the decrease of octahedral vibrational frequency. This may be the reasons for the increase in the octahedral peak intensity. The increase in the concentration of Fe^{3+} ions having lower ionic radius and lower atomic weight in the tetrahedral site increases the tetrahedral frequency vibration. All our samples show a split in the octahedral frequency band. Priyadarsini et al.¹³ have obtained similar split in the octahedral frequency band.

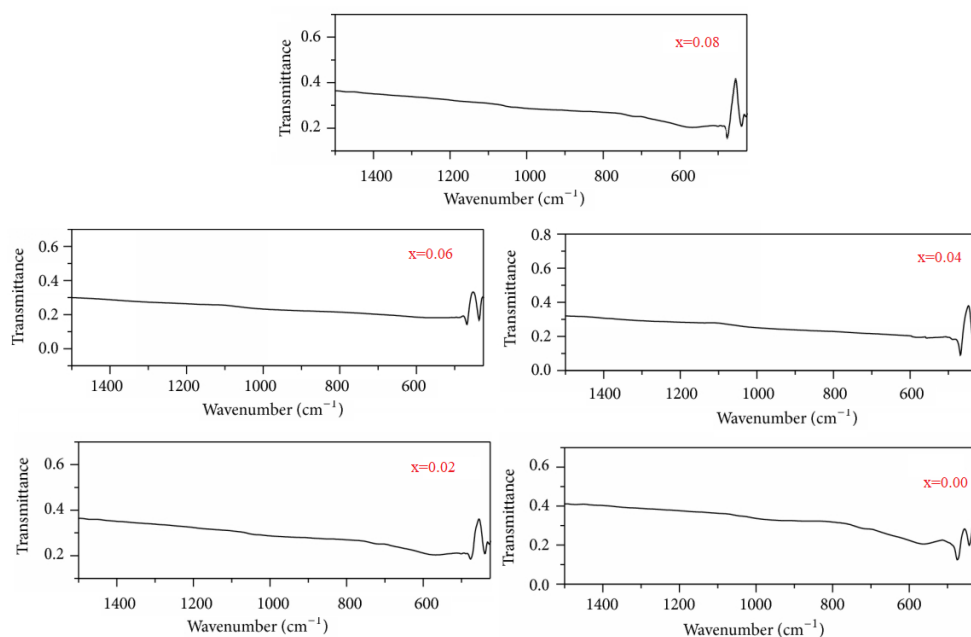


Figure 3: FTIR spectra of $\text{Mn}_{0.2}\text{Ni}_{0.6}\text{Zn}_{0.5}\text{Ce}_x\text{Fe}_{(2-x)}\text{O}_4$ (where $x = 0.00, 0.02, 0.04, 0.06, 0.08$)

Surface morphology by SEM study

The surface morphology of the Mn-Ni-Zn nanoferrite particles doped with Ce^{3+} was examined by scanning electron microscopy (SEM) shown in Figure 4 which indicates the agglomerated nanoparticles which is attributed to the magnetic exchange interaction between the nanoparticles. It is observed that the average particle size of the prepared samples goes on increasing on substitution of Ce^{3+} in the place of Mn and Fe in ferrites. The average grain size of all the prepared samples directly calculated from SEM instrument is in the range of 30-40nm only. The SEM images of samples and with/without Ce^{3+} addition ($x=0.0$ to 0.08) were shown in Figure 4. SEM image of the sample Mn-Ni-Zn doped with Cerium shows good homogeneity.

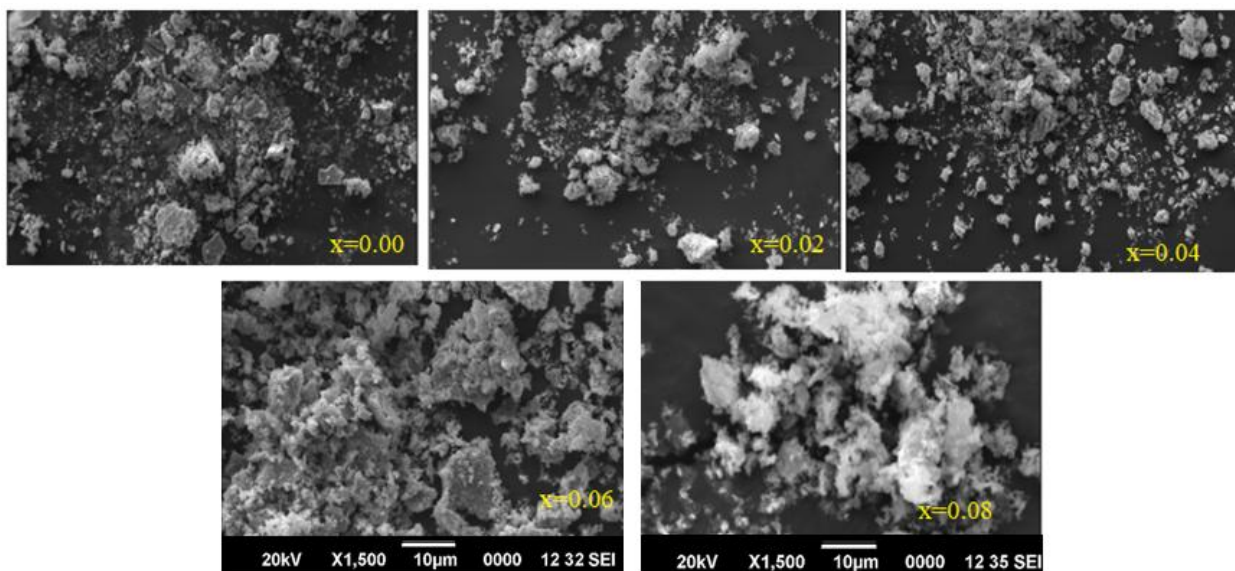


Figure 4: SEM images of $\text{Mn}_{0.2}\text{Ni}_{0.6}\text{Zn}_{0.5}\text{Ce}_x\text{Fe}_{(2-x)}\text{O}_4$ (where $x = 0.00, 0.02, 0.04, 0.06, 0.08$)

Magnetic Properties

Magnetization measurements were carried out on a vibrating sample magnetometer at room temperature with a maximum applied field of 20kOe. Figure 5 shows the typical magnetic hysteresis loops of system. The saturation magnetization, coercivity, and remnant ratio of all the samples are presented in Table 2.

Table 2: Effect of Ce^{3+} doping on magnetic parameters of $Mn_{0.2}Ni_{0.6}Zn_{0.5}Ce_xFe_{(2-x)}O_4$ (where $x=0.00, 0.02, 0.04, 0.06, 0.08$)

Ce^{3+} substituted Nanoferrites (x)	M_s (emu/g)	M_r (emu/g)	$H_c(O_e)$	R
$Mn_{0.2}Ni_{0.6}Zn_{0.5}Fe_2O_4$	53.28	20.47	1406.78	0.3919
$Mn_{0.2}Ni_{0.6}Zn_{0.5}Ce_{0.02}Fe_{(2-0.02)}O_4$	38.38	15.88	1226.86	0.4221
$Mn_{0.2}Ni_{0.6}Zn_{0.5}Ce_{0.04}Fe_{(2-0.04)}O_4$	37.38	12.24	1076.61	0.3339
$Mn_{0.2}Ni_{0.6}Zn_{0.5}Ce_{0.06}Fe_{(2-0.06)}O_4$	32.85	12.02	1045.50	0.3730
$Mn_{0.2}Ni_{0.6}Zn_{0.5}Ce_{0.08}Fe_{(2-0.08)}O_4$	36.30	12.90	991.68	0.3625

The saturation magnetization value decreases from 53.28 to 32.55 emu/g with the increase in cerium content from 0.0 to 0.08. The value of at room temperature for the pure Manganese ferrite sample is 53.28 emu/g. The low value of saturation magnetization compared with that of the bulk can be understood on the basis of core-shell model, which explains that the finite size effects of the nanoparticles lead to canting or noncollinearity of spins on their surface and thereby reduce magnetization¹⁴.

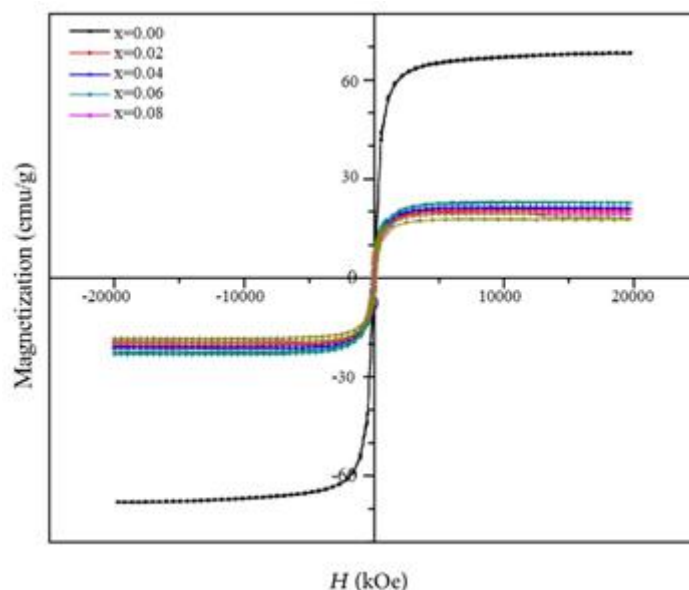


Figure 5: Room temperature hysteresis curves of $Mn_{0.2}Ni_{0.6}Zn_{0.5}Ce_xFe_{(2-x)}O_4$ (where $x=0.00, 0.02, 0.04, 0.06, 0.08$)

The net magnetic moment in the ferrite materials depends on the number of magnetic ions occupying the tetrahedral and octahedral sites. The magnetic moments of rare earth ions generally originate from the localized 4f electrons, and they are characterized by lower ordering temperatures, that is, less than 40 K¹⁵. Therefore, the effect of rare-earth atoms in the Mn ferrite materials seems to be similar to the substitution of nonmagnetic atoms in the octahedral Fe sites of the spinel lattices. It is expected that the magnetization will be proportional to the effective magnetic moment of Ce^{3+} ions. But the substitution of Fe^{3+} ions by Ce^{3+} ions in the octahedral site decreases $Fe^{3+}-Fe^{3+}$ interactions. So the magnetization is decreased because of the decrease of the strong $Fe^{3+}-Fe^{3+}$ interactions. Therefore, Cerium substitution can be considered as a nonmagnetic ion substitution in octahedral B-site and this reduces the exchange interaction between octahedral and tetrahedral sites, which results in the decrease of magnetization.

The coercivity which measures the magnetic field strength required for overcoming anisotropy to flip the magnetic moments is clearly affected by the Ce³⁺ substitution. It is reported that coercivity is affected by the factors such as magneto crystallinity, microstrain, size distribution, anisotropy, and the magnetic domain size¹⁶. The coercivity values of the Cerium-substituted Manganese ferrite samples vary from 1406.78 to 991.68 Oe. These values are much greater than that reported for rare earth-substituted Manganese ferrite samples synthesized by other methods¹⁷. It is reported that, in the multidomain regime, the coercivity is inversely proportional to the grain size¹⁸. A larger grain size makes the motion of domain walls easier, and thereby the coercivity decreases. This may be the reason for the decrease in the coercivity with the increase in Ce³⁺ ion content. The remnant ratio is an indication of the ease with which the direction of magnetization reorients to the nearest easy axis magnetization direction after the magnetic field is removed. The values of remnant ratio of the prepared samples are in the range from 0.33 to 0.42. This is an indication of decrease in anisotropy of the crystal lattice¹⁹.

Conclusion

A series of samarium-substituted manganese ferrites, with , 0.0, 0.02, 0.04, 0.06 and 0.08 were synthesized by using sol-gel method. XRD analysis confirmed the formation of single-phase spinel structure, without any secondary phase in all the compositions. The substitution of Cerium in Manganese ferrite has resulted in an increase in lattice parameter and crystallite size. The decrease in lattice parameter for indicates a possible cationic redistribution. The low values of the lattice strain induced due to Ce³⁺ doping indicate improved crystallinity of the sample. The absorption bands in FTIR spectra of all the samples are found in the expected range. The band frequencies decrease with increase in cerium content and this suggests the occupancy of Ce³⁺ ions on the octahedral sites. The saturation magnetization decreased with an increase in Ce³⁺ content and this is attributed to the decrease in the net magnetic moment due to the substitution of nonmagnetic ion in the octahedral site. The change in coercivity with Ce³⁺ content is explained based on the variation of coercivity of nanoparticles in the multidomain regime. These investigations suggest that the properties of the Manganese ferrite nanoparticles substituted with Ce³⁺ ions can be tailored for suitable applications.

Reference

- 1 Chen D, Liu HY, Li L. One-step synthesis of manganese ferrite nanoparticles by ultrasonic wave-assisted ball milling technology. *Materials Chemistry and Physics*. 2012;134(2-3):921-924.
- 2 Y L N Murthy, I V Kasi Viswanath, T. Kondala Rao, Rajendra Singh., Synthesis and characterization of Nickel Copper Ferrite, *International Journal of ChemTech Research* 2009 ,Vol.1, No.4, pp 1308-1311.
- 3 Amarendra KS, Goel TC, Mendiratta RG. Magnetic properties of Mn-substituted Ni-Zn ferrites. *J Appl Phys* 2002;92:3872-6
- 4 Sattar AA, El-Sayed HM, El-Shokrofy KM, El-Tabey MM. Effect of manganese substitution on the magnetic properties of nickel-zinc ferrite. *J Mater Eng and Perform* 2005;14(1):99-103
- 5 Kulkarni Suresh R. Development of In³⁺ substituted Mn-Ni-Zn nanoferrite core material. *Arch Phys Res* 2012;3(2):116-22.
- 6 Choi WO, Kwon WH, Lee JG, Kang BS, Chae KP. Structural and magnetic properties of nanoparticle Mn-Zn-Ni ferrite powders grown by using a sol-gel method. *J Korean Phys Soc* 2012;61(11):1812-6
- 7 Sattar AA, El-Sayed HM, Agami WR. Physical and magnetic properties of calcium-substituted Li-Zn ferrite. *J Mater Eng Perform* 2007;16:573-7.
- 8 Sattar AA, Wafik AH, El-Sayed HM. Infrared spectra and magnetic studies of trivalent doped Li-ferrites. *Phys Status Solidi a* 2001;186(3):415-22.
- 9 M. Kaiser, "Effect of preparation condition on nickel zinc ferrite nanoparticle: a comparison between sol-gel," *Journal of Alloys and Compounds*, vol. 468, no. 1-2, pp. 15-21, 2009.
- 10 R. D. Waldron, "Infrared spectra of ferrites," *Physical Review*, vol. 99, no. 6, pp. 1727-1735, 1955

- 11 R. K. Puri and U. Varshney, "Mössbauer study of Zn²⁺ and Sn⁴⁺ additives in Nickel ferrites," *Journal of Physics and Chemistry of Solids*, vol. 44, no. 7, pp. 655–661, 1983.
- 12 C. Venkataraju, G. Sathishkumar, and K. Sivakumar, "Effect of cation distribution on the structural and magnetic properties of nickel substituted nanosized Mn-Zn ferrites prepared by co-precipitation method," *Journal of Magnetism and Magnetic Materials*, vol. 322, no. 2, pp. 230–233, 2010
- 13 P. Priyadharsini, A. Pradeep, P. S. Rao, and G. Chandrasekaran, "Structural, spectroscopic and magnetic study of nanocrystalline Ni-Zn ferrites," *Materials Chemistry and Physics*, vol. 116, no. 1, pp. 207–213, 2009.
- 14 P. Priyadharsini, A. Pradeep, P. S. Rao, and G. Chandrasekaran, "Structural, spectroscopic and magnetic study of nanocrystalline Ni-Zn ferrites," *Materials Chemistry and Physics*, vol. 116, no. 1, pp. 207–213, 2009.
- 15 R. N. Panda, J. C. Shih, and T. S. Chin, "Magnetic properties of nano-crystalline Gd- or Pr-substituted CoFe₂O₄ synthesized by the citrate precursor technique," *Journal of Magnetism and Magnetic Materials*, vol. 257, no. 1, pp. 79–86, 2003.
- 16 J. Jing, L. Liangchao, and X. Feng, "Structural analysis and magnetic properties of Gd-doped Li-Ni ferrites prepared using rheological phase reaction method," *Journal of Rare Earths*, vol. 25, no. 1, pp. 79–83, 2007.
- 17 M. M. Rashad, R. M. Mohamed, and H. El-Shall, "Magnetic properties of nanocrystalline Sm-substituted CoFe₂O₄ synthesized by citrate precursor method," *Journal of Materials Processing Technology*, vol. 198, no. 1–3, pp. 139–146, 2008
- 18 S. Chakraverty and M. Bandyopadhyay, "Coercivity of magnetic nanoparticles: a stochastic model," *Journal of Physics Condensed Matter*, vol. 19, no. 21, Article ID 216201, 2007
- 19 S. E. Shirsath, B. G. Toksha, and K. M. Jadhav, "Structural and magnetic properties of In³⁺ substituted NiFe₂O₄," *Materials Chemistry and Physics*, vol. 117, no. 1, pp. 163–168, 2009.